LETTER Communicated by Bard Ermentrout

Oscillatory Synchronization Requires Precise and Balanced Feedback Inhibition in a Model of the Insect Antennal Lobe

Dominique Martinez
dmartine@loria.fr
LORIA-CNRS Vandoeuvre-Les-Nancy 54506, France

In the insect olfactory system, odor-evoked transient synchronization of antennal lobe (AL) projection neurons (PNs) is phase-locked to the oscillations of the local field potential. Sensory information is contained in the spatiotemporal synchronization pattern formed by the identities of the phase-locked PNs. This article investigates the role of feedback inhibition from the local neurons (LNs) in this coding. First, experimental biological results are reproduced with a reduced computational spiking neural network model of the AL. Second, the low complexity of the model leads to a mathematical analysis from which a lower bound on the phase-locking probability is derived. Parameters involved in the bound indicate that PN phase locking depends not only on the number of LN-evoked inhibitory postsynaptic potentials (IPSPs) previously received, but also on their temporal jitter. If the inhibition received by a PN at the current oscillatory cycle is both perfectly balanced (i.e., equal to the mean inhibitory drive) and precise (without any jitter), then the PN will be phase-locked at the next oscillatory cycle with probability one.

1 Introduction

Oscillations are often observed in recorded electrical signals such as electroencephalograms (EEGs) or local field potentials (LFPs) (Buzsaki & Draguhn, 2004; Wang, 2003; Kopell, 2003). These oscillations seem to play an important role in the coding of sensory information by providing a "clock" or temporal frame of reference for the encoding neurons. In the hippocampus of rats, for example, place cells exhibit phase-dependent firing activity relative to the EEG theta oscillation (O'Keefe 1993; Huxter, Burgess, & O'Keefe, 2003). In the olfactory system of insects, antennal lobe projection neurons are phase-locked to the LFP oscillation (Laurent, Wehr, & Davidowitz, 1996). Several studies have shown that inhibitory feedback shapes oscillatory synchronization (e.g., Wang & Buzsaki, 1996; Whittington, Traub, Kopell, Ermentrout, & Buhl, 2000; Börgers & Kopell, 2003). These studies, however, have focused on macroscopic network properties, such as the emergence of oscillations and global synchronization, and did not consider the fact that some neurons exhibit phase-locked activity

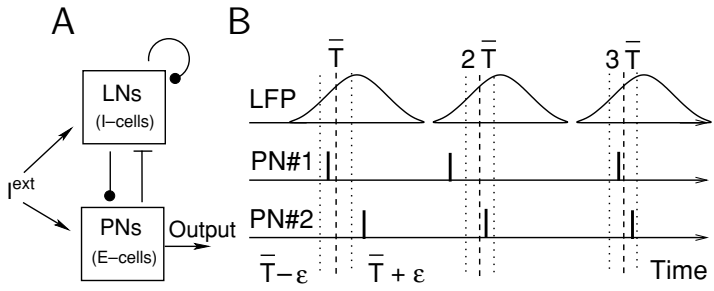

Figure 1: (A) The insect AL as an excitatory-inhibitory network. Local neurons (LNs) are inhibitory cells (I-cells) and projection neurons are excitatory cells (E-cells). Although connections between PNs may be present in the locust, they do not seem to play a significant role on PN phase locking (Bazhenov et al., 2001b) and for simplicity are not considered in our AL model. (B) PN phase locking. The LFP is recorded in the mushroom body, a higher structure where the PNs project. The oscillations of the LFP define a "clock" of a 50 ms period corresponding to 20 Hz oscillations for the locust AL. Ticks depict individual PN spikes. Phase-locked PNs fire in the ascending phase of the mushroom body LFP with a consistent phase lag of -70° (Laurent & Davidowitz, 1994) corresponding to a mean firing time $\overline{T}$ of the PN population occurring approximately 10 ms before the peak of the LFP. This phase lag is probably due to the conduction time between the AL and the mushroom body (see chapter 4 in Perez-Orive, 2004). We consider that phase-locked PNs are those that fire within a temporal window of $\pm\epsilon$ ms around the PN mean firing time $\overline{T}$, typically $\epsilon = 5$ ms (Laurent, 1999; Laurent et al., 2001). If one assigns bit 1 or 0 to phase-locked or non-phase-locked PNs (see, e.g., Laurent, 1996), then the population vectors formed by PN#1 and 2 and the three oscillatory cycles are (10, 01, 11).

while others do not. How does the received inhibition affect the probability of individual neurons to be phase-locked to the simultaneously recorded field potential? To address this question, we use a simplified computational model of the insect AL that allows analytic calculations.

The first structure of the insect olfactory system, the AL, is formed by a small network of excitatory PNs and inhibitory LNs (see Figure 1A). Only PNs project to the mushroom body, a higher brain structure where the LFP is recorded. In the presence of an olfactory stimulus, subsets of PNs fire in synchrony, giving rise to LFP oscillations in the mushroom body. Neither global properties of the LFP oscillatory activity (e.g., the mean frequency) nor the phase of the PN or LN activity relative to the LFP have been found to convey information about odor identity (Laurent, 1996; Friedrich, Habermann, & Laurent, 2004) and intensity (Stopfer, Jayaraman, & Laurent, 2003). In contrast, the identities of the phase-locked PNs evolve in time in an odor-specific manner (Laurent & Davidowitz, 1994; Laurent et al., 1996;

Wehr & Laurent, 1996; Laurent, 1999). Figure 1B clarifies the significance of phase locking in this context. Both experimental and modeling studies support the functional relevance of fast LN-PN inhibition in this coding. First, when the GABAergic synapses are pharmacologically blocked, synchronization is disrupted, and insects are no longer able to discriminate between similar odors (Stopfer, Bhagavan, Smith, & Laurent, 1997; Hosler, Buxton, & Smith, 2000). Second, a recent biologically detailed model of the locust AL has shown that LN-mediated inhibition can effectively control the transient synchronization of the PNs (Bazhenov et al., 2001b). This model, however, is difficult to analyze mathematically because of its high complexity. We propose a simplified computational spiking neural network AL model that leads to analytic calculations concerning the role of feedback LN-PN inhibition on PN phase locking. In section 2, we show that our model reproduces the transient synchronization patterns observed in modeling and experimental studies (Wehr & Laurent, 1996; Bazhenov et al., 2001b). In section 3, we derive a lower bound on the PN phase-locking probability. In section 4, we demonstrate the validity of this bound with simulation results.

2 A Simplified Computational Spiking Neural Network Model of the Insect AL

2.1 Description of the Model. Our AL model is built on earlier work from Bazhenov et al. (2001b). It is a sparsely and randomly connected network of theta neurons (Ermentrout, 1996; Hoppenstead & Izhikevich 2002) coupled via simple exponential synapses.

The state variable θ of a theta neuron obeys the following equation,

$$\frac{d\theta}{dt} = (1 - \cos\theta) + (1 + \cos\theta)\alpha J, \tag{2.1}$$

where J is the total input current and $\alpha > 0$ is a constant characterizing the neuron current-frequency response curve. Such a theta neuron can be considered as a point $(\cos\theta, \sin\theta)$ moving on the unit circle (Ermentrout, 1996, Hoppenstead & Izhikevich, 2002) for which a spike occurs whenever θ crosses π. When $J > 0$ and constant, the neuron fires regularly at a frequency given by $\sqrt{\alpha J}/\pi$. By using the transformation $v = \tan(\theta/2)$, the theta model becomes the quadratic integrate-and-fire model.

The schematic architecture of our AL network is depicted in Figure 1A. We did not consider interconnections between PNs because they have a negligible influence in both our model and Bazhenov et al. (2001b). Thus, the only synaptic current of a PN comes from the LNs and is given by

$$I_{PN}^{syn}(t) = -g \sum_i H\big(t - t_i^f\big) e^{-(t-t_i^f)/\tau}, \tag{2.2}$$

where H is the Heaviside function, $g \geq 0$ and τ are the strength and the time constant of the inhibitory synapses, respectively, and t_i^f, $i = 1, 2, \cdots$, is the set of firing times of all the LNs that project to this particular PN. For clarity, details about the model are omitted here, and we refer to section A.1 in the appendix for a detailed justification of the parameters used in the model regarding the neurons, the network, and the stimulus.

2.2 Simulation of the Model. In the presence of a stimulus, the network shows the following repeated characteristic behavior: a quasi-synchronized PN spike volley followed immediately by a similar LN spike volley and a silent period (see Figure 2A). In subplot j, each PN spike is represented by a dot whose size indicates the amount of inhibition the PN has received at the previous oscillatory cycle. In the simulations performed, the PNs receiving zero or one IPSP are not phase-locked. Moreover, dividing the strength of the inhibitory LN-PN synapses by a factor of 10 resulted in a loss of PN synchronization and LFP oscillation (see Figure 2B). Therefore a strong inhibitory feedback from the LNs is necessary for oscillatory synchronization to take place.

In order to study the role of feedback inhibition, we adapted the analysis reported by Laurent et al. (1996) and Bazhenov et al. (2001b), by assigning to each PN spike a phase $(-\pi, +\pi)$ relative to its closest LFP peak (zero phase = positive peak of the LFP). Note that the LFP is artificially generated in our simulations as the average of the PNs' θ variables so that there is no phase lag between the peak of the LFP and the mean firing time $\overline{T}$ of the PN population. Figure 3 shows the results of this analysis for 20 different runs of the AL network and a particular PN (see the Figure 3 caption for details). Transient synchronization of the PN relative to the LFP oscillation can be seen in Figure 3 at the top. Clearly, the PN fires precisely and is phase-locked with the second, third, fourth, and tenth oscillatory cycles, whereas it is not with the other cycles. As in Wehr and Laurent (1996), the output of this PN can be represented as the binary vector (0, 1, 1, 1, 0, 0, 0, 0, 0, 1), in which the kth bit corresponds to synchronization or desynchronization at the kth oscillatory cycle. Depending on their particular connectivity with the set of active LNs, different PNs show different patterns of synchronization. Time evolution in these patterns is induced by a change over time in the PNs' inhibitory drive (see Figure 3, second row). As in Bazhenov et al. (2001b), lateral inhibition and firing-rate adaptation leads to a complex competition between LNs in our network so that the LNs that are active at a given oscillatory cycle are not necessarily the same as those activated at other cycles (see Figure 2A). To illustrate this effect, we reran simulations without any LN firing-rate adaptation. In this condition, the subset of active LNs no longer changes (see Figure 2C). As a consequence of the fixed inhibitory drive, the subset of phase-locked PNs becomes time invariant, a PN being either synchronized or desynchronized at all oscillatory cycles (see Figure 4).

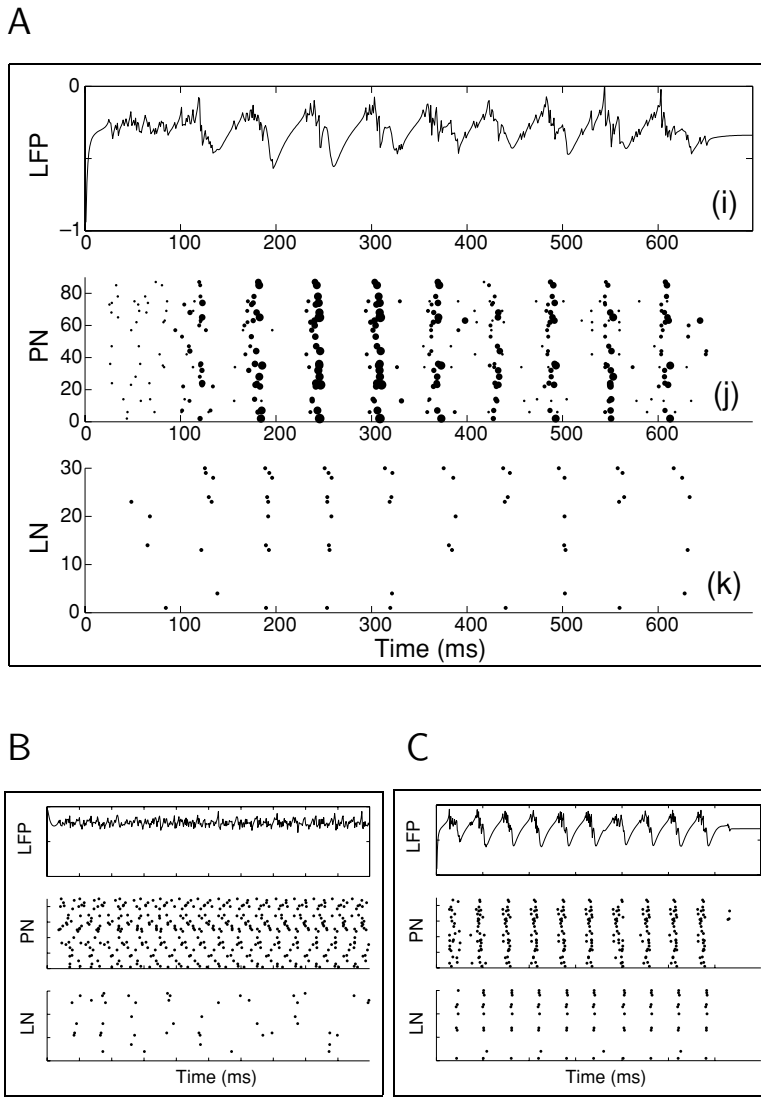

Figure 2: Simulations of our AL model (30 LNs and 90 PNs). (A) Corresponds to the simulation of an intact network. Subplot i represents the time evolution of the LFP (the LFP is taken as the average of the PNs' variables θ). Subplot j is the raster plot of the PN spikes (the size of a dot is proportional to the number of LN-evoked IPSPs received by the PN at the previous oscillatory cycle). Subplot k is the raster plot of the LN spikes. (B) Corresponds to the simulation of a network with weak inhibitory LN-PN synapses. (C) Corresponds to the simulation of a network without LN firing-rate adaptation.

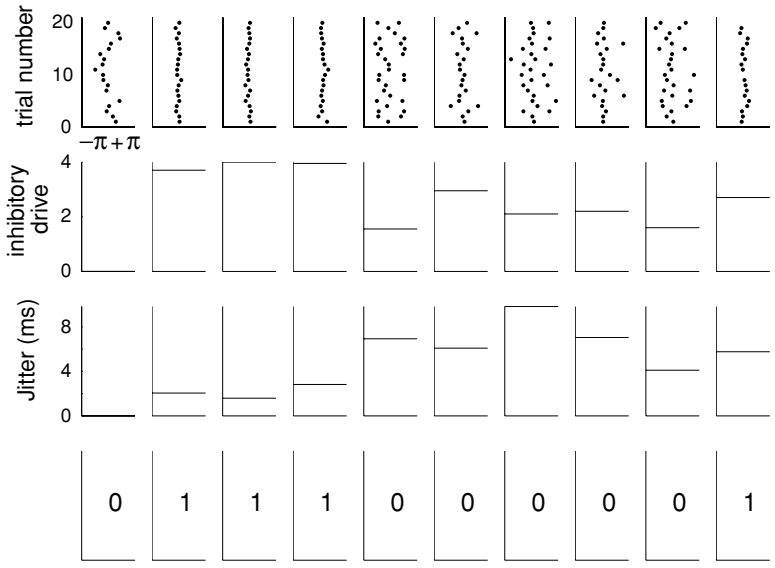

Figure 3: Temporal analysis of PN#1 over 20 simulations of the 90-30 network with different initial conditions $\theta(t = 0)$ and different input currents due to the noise. For repeated trials, the stimulus was applied to the same 33% "random set" of neurons. Each column corresponds to a given oscillatory cycle (from 1 to 10). The first row at the top shows the phase of each PN spike relative to its closest peak of the LFP (the phase of a given spike relative to the ith peak of the LFP is plotted as a dot in the ith box). The second row shows the inhibitory drive: the mean number of LN-evoked IPSPs received by PN#1 at the previous oscillatory cycle. The third row shows the standard deviation of the temporal jitter (in ms) of these LN-evoked IPSPs. Inhibitory drive and temporal jitter are estimated as averages over the 20 runs. The fourth row, at the bottom, represents the binary code obtained by assigning $+1$ at the ith bit if at least 80% of the spikes belonging to the ith box are within a ± 5 ms windows around the ensemble mean of the PN population.

This stable state is reached very quickly, after just one oscillatory cycle. The number of phase-locked PNs increases with the probability p of connection and the number of activated neurons, which reflects the odor concentration (model assumption in section A.1). As an example, about 24% of the PNs are phase-locked when the odor activates 33% of the neurons and $p = 0.3$. As shown in Figure 4, a phase-locked PN produces a single spike per oscillatory cycle, and the phase-locking pattern is reproducible across repeated trials, in agreement with previous work (Laurent, 1996; Wehr & Laurent, 1996).

These observations confirm that our model can reproduce the transient synchronization patterns seen in both experimental data (Wehr & Laurent,

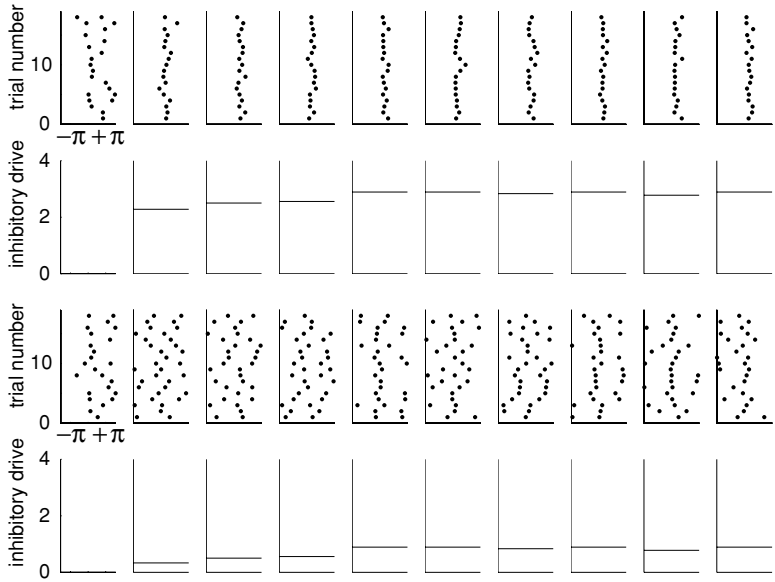

Figure 4: Network without LN firing-rate adaptation. When LN frequency adaptation is blocked, the subset of phase-locked PNs becomes time invariant, a PN being either synchronized or desynchronized at all oscillatory cycles. The first two rows at the top are for a phase-locked PN. The last two rows at the bottom are for a desynchronized PN. Each box corresponds to an oscillatory cycle (from 1 to 10). The phase of each spike is represented as a dot across repeated trials. The inhibitory drive is the mean number of IPSPs received by the neuron at the previous oscillatory cycle estimated as the average over 20 trials.

1996) and the original model of Bazhenov et al. (2001b). Furthermore, as seen in Figure 3 (second and third rows), the synchronization of a PN to the current cycle seems to depend not only on the number of inhibitory spikes received at the previous cycle, as suggested by Bazhenov et al. (2001b), but also on the temporal jitter in their arrival times. This point is developed in the next section.

3 Mathematical Analysis

3.1 Firing Times of Inhibited PNs. The previous simulations suggest that the firing time of a PN is constrained by the inhibition it has previously received. We first consider a PN receiving a single inhibitory postsynaptic potential of strength g at a time t^f. From equation 2.2 and section A.1, the total input current, for $t \geq t^f$, is given by

$$J(t) = I - ge^{-(t-t^f)/\tau},$$

where τ is the synaptic decay time and $I = I^{ext} - I^{th}$ (for PNs, $I^{adapt} = 0$). The PN is not allowed to fire until the inhibition has worn away sufficiently so that the total input current becomes positive. Börgers and Kopell (2003) have shown that the firing time T_1 of a theta neuron receiving a single strong inhibitory spike is relatively independent of the initial condition $\theta(t = 0)$. Provided g is large enough, trajectories in the phase plane (θ, J) are all attracted toward a given trajectory so that they all reach approximately the same point $(\pi, J^\star)$ at firing time (see Figure 5C in Börgers & Kopell, 2003 for an illustration). The result is an almost complete loss of the initial condition $\theta(t = 0)$. Whatever the initial condition might be, the total input current is approximately equal to $J^\star$ at the firing time T_1,

$$J^\star \approx J(T_1) = I - ge^{-(T_1 - t^f)/\tau},$$

and thus

$$T_1 \approx \tau \ln g - \tau \nu(I) + t^f,$$

where $\nu(I) = \ln(I - J^\star)$. In order to obtain expressions for the firing time of a PN, we have generalized Börgers and Kopell's (2003) study to the case of a theta neuron receiving k strong inhibitory spikes of strength g at times t_i^f, $i = 1 \cdots k$, as in equation 2.2. Without loss of generality, we consider that the neuron fires after t_k^f. At the firing time T_k, the total input current is approximately equal to $J^\star$,

$$J^\star \approx J(T_k) = I - \sum_{i=1}^{k} ge^{-(T_k - t_i^f)/\tau},$$

and thus the firing time of a PN that received k inhibitions is

$$T_k \approx \tau \ln(kg) - \tau \nu(I) + \tau \ln \frac{1}{k} \sum_{i=1}^{k} e^{t_i^f/\tau}. \tag{3.1}$$

Note that by using Jensen's inequality, one obtains

$$T_k \geq \tau \ln(kg) - \tau \nu(I) + <t^f>,$$

which means that T_k is larger than the synchronization time of the population receiving a single spike of strength kg at the mean time $<t^f> = \frac{1}{k} \sum_{i=1}^{k} t_i^f$.

Let us consider that the firing times t_i^f of the LNs are drawn randomly from an unknown probability density function with mean μ_{LN} and standard deviation σ_{LN}. The only random variable in equation 3.1 is thus

$$X = \tau \ln \frac{1}{k} \sum_{i=1}^{k} e^{t_i^f/\tau},$$

where the mean and standard deviation are given by $\overline{X} \approx \mu_{LN}$ and $\sigma_X \approx \sigma_{LN}/\sqrt{k}$. These expressions for $\overline{X}$ and σ_X were found by considering the fact that the variance of the sum of k independently and identically distributed (i.i.d.) random variables, each with variance σ^2, is $k\sigma^2$, and that the mean and standard deviation of a function $y = g(x)$ of a random variable x approximately depend on only the mean η_x and standard deviation σ_x of x : $\eta_y \approx g(\eta_x)$ and $\sigma_y \approx |dg/dx|_{x=\eta}\sigma_x$ (Papoulis, 1984, eq. 5-53 and 5-56).

Therefore, the firing times of the PNs that received k inhibitions are randomly distributed with variance

$$E[(T_k - \overline{T}_k)^2] = \sigma_X^2 \approx \frac{\sigma_{LN}^2}{k} \tag{3.2}$$

and mean

$$\begin{aligned} \overline{T}_k &\approx \tau \ln(kg) - \tau\nu(I) + \overline{X} \\ &= \overline{T}_1 + \tau \ln k, \end{aligned} \tag{3.3}$$

where $\overline{T}_1$ is the mean firing time of a PN that received a single LN inhibitory spike,

$$\overline{T}_1 \approx \tau \ln(g) - \tau\nu(I) + \mu_{LN}. \tag{3.4}$$

3.2 Phase-Locking Probability of Inhibited PNs. As we have seen in section 2, PNs that do not receive any inhibition are not phase-locked. Therefore, we consider here only the PNs that receive some amount of inhibition. The mean firing time of these inhibited PNs is $\overline{T} = E[T]$, where E is the expected value taken over the probability density function $f_T(T)$. Because a PN receives at each oscillatory cycle a discrete number of LN-evoked IPSPs, the probability density function of its firing time $f_T(T)$ can be expressed as a mixture of conditional densities,

$$f_T(T) = \sum_{k \geq 1} p_k f_T(T|k),$$

where p_k is the probability that an inhibited PN receives exactly k inhibitions

and $f_T(T|k)$ is the conditional density of firing time T given k LN-caused IPSPs. (Expression for p_k is given in section A.2.) From the above mixture model, $\overline{T}$ is given by

$$\overline{T} = \sum_{k\geq 1} p_k \overline{T}_k. \tag{3.5}$$

Replacing equation 3.3 in 3.5 yields

$$\begin{aligned}\overline{T} &\approx \overline{T}_1 + \tau \sum_{k\geq 1} p_k \ln k \\ &\approx \overline{T}_1 + \tau \ln <k>,\end{aligned} \tag{3.6}$$

where $<k>$ is the mean inhibitory drive. For our model, we have $<k> = p\, N^a_{LN}$ with p the probability of connection and N^a_{LN} the number of active LNs. Approximation in equation 3.6 is obtained by considering $E[\ln k] \approx \ln E[k]$ for k concentrated near its mean. This is a valid assumption here because the variance of k corresponds to $p(1-p)N^a_{LN}$, which is small because N^a_{LN} is not too large.

We further consider that a PN receiving k LN-evoked IPSPs at the current oscillatory cycle will be phase-locked at the next cycle if its firing time T_k is within a temporal window of $\pm\epsilon$ ms around the ensemble mean $\overline{T}$ (see also Figure 1B). The Chebychev inequality provides a lower bound on the probability that an inhibited PN is phase-locked,

$$P(|T_k - \overline{T}| < \epsilon) \geq 1 - \frac{E[(T_k - \overline{T})^2]}{\epsilon^2}. \tag{3.7}$$

Using equations 3.2, 3.3, and 3.6, it can be shown that

$$\begin{aligned}E[(T_k - \overline{T})^2] &= E[(T_k - \overline{T}_k)^2] + (\overline{T}_k - \overline{T})^2 \\ &\approx \frac{\sigma^2_{LN}}{k} + \tau^2 \left(\ln \frac{k}{<k>}\right)^2.\end{aligned} \tag{3.8}$$

Equations 3.7 and 3.8 provide a lower bound on the probability that a PN receiving exactly k inhibitions is phase-locked. The first and second terms in the right-hand side of equation 3.8 represent the contribution of the temporal jitter σ_{LN} and the number k of LN-evoked IPSPs at the previous oscillatory cycle, respectively. The received inhibition is said to be precise when σ_{LN} is small, such that the first term in equation 3.8 can be neglected. The inhibition is said to be balanced when k is near the mean inhibitory drive $<k>$, such that the second term in equation 3.8 can be neglected. When the inhibition is both balanced and precise, then the phase-locking probability is close to one.

The temporal jitter of the PNs spikes is given with equation 3.8 and

$$\sigma_{PN}^2 = \sum_{k=1}^{N_{LN}^a} p_k E[(T_k - \overline{T})^2]. \tag{3.9}$$

An alternate expression for σ_{PN}^2 is found by considering the number k of received IPSPs as a random variable with mean $<k>$ and variance σ_k^2. In equation 3.1, we now have a sum of a random number k of independent random variables (recall that the times of single IPSPs are independent random variables, with variance σ_{LN}^2). By applying the formulas of the variance of a random sum and of a function, we found

$$\sigma_{PN}^2 \approx \frac{\sigma_{LN}^2}{<k>} + \tau^2 \frac{\sigma_k^2}{<k>^2}. \tag{3.10}$$

We see that σ_{PN}^2 vanishes when the received inhibition is both perfectly balanced ($k = <k>, \sigma_k^2 = 0$) and precise ($\sigma_{LN}^2 = 0$), indicating perfect synchronization of the PN population. When the inhibition is balanced for all the PNs, then $p_k = 1$ for $k = <k>$ and $p_k = 0$ otherwise, so that equations 3.9 and 3.8 together become equivalent to equation 3.10 with $\sigma_k^2 = 0$. When the inhibition is precise, equation 3.10 with $\sigma_{LN}^2 = 0$ is similar to equation 4.20 in Börgers and Kopell (2003).

4 Numerical Results

The bound derived in equations 3.7 and 3.8 allows one to predict which PNs will be phased-locked at the next oscillatory cycle and which will not. This prediction requires only knowledge of the number and the jitter of the IPSPs received by individual PNs at the current LFP oscillation. It depends, however, on a specific choice for ϵ. Experimental observations suggest that phase-locked PN spikes occur within a ± 5 ms window (Laurent, 1999; Laurent et al., 2001). PN spikes are received by Kenyon cells (KCs) in the mushroom body. As shown in section A.3, the estimated firing probability for a KC receiving PN spikes within a ± 5 ms window is close to the one experimentally found in (Perez-Orive et al., 2002). Therefore, in the following, we choose $\epsilon = \pm 5$ ms to determine whether a PN is phase-locked.

As shown in Figure 5, the phase-locking probability given by equations 3.7 and 3.8 when $\sigma_{LN} = 0$ is an asymmetric bell-shaped function centered on the mean inhibitory drive $<k>$. We consider that a given PN is phase-locked when this probability is higher than a given threshold P_{th}. It is easy to check that this will happen for $k \in (<k> \exp(-\epsilon\sqrt{1 - P_{th}}/\tau), <k> \exp(\epsilon\sqrt{1 - P_{th}}/\tau))$. For the values used in our AL model—$\tau = 10$ ms and $\epsilon = 5$ ms—and for $P_{th} = 0.3$, a threshold value was taken from Wehr and Laurent (1996), we obtain $k \in (0.66 <k>, 1.52 <k>)$. Clearly, the range of

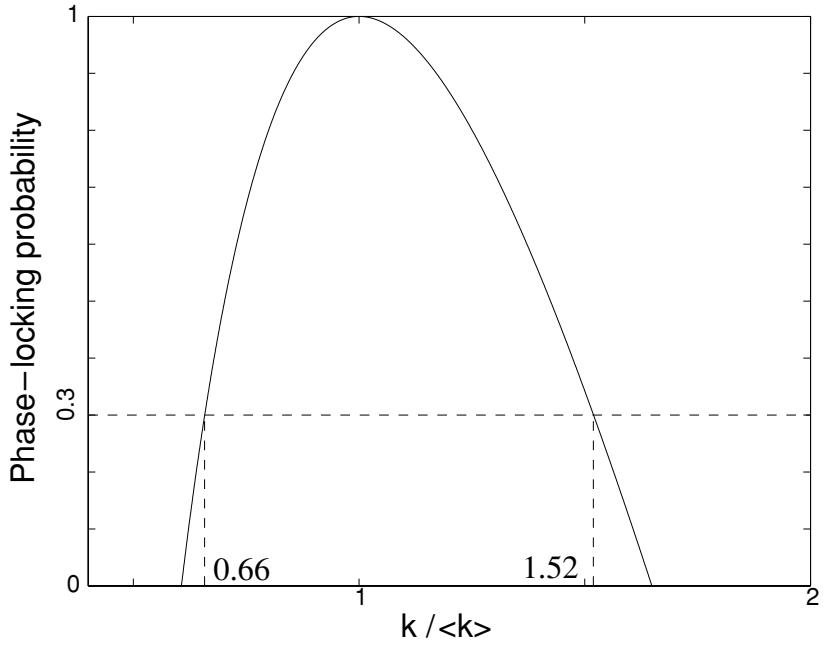

Figure 5: Phase-locking probability versus deviation from mean inhibition. In case of precise inhibition ($\sigma_{LN} = 0$), the phase-locking probability, given by equations 3.7 and 3.8, is an asymmetric bell-shaped function centered on the mean inhibitory drive $<k>$ received by the PNs at the previous oscillatory cycle. We consider that a PN is phase-locked if this probability is higher than 0.3 (Wehr & Laurent, 1996), which gives a synchronization range of $k \in (0.66 <k>, 1.52 <k>)$.

inhibitory drive k that allows PN phase locking grows with the mean inhibition $<k>$. Therefore, PNs are more likely to be synchronized when a large number of LNs are active in the network.

Figure 6A compares the lower bound (see equations 3.7 and 3.8) to the phase-locking probability estimated by the simulation of our AL model. The lower bound was computed using equations 3.7 and 3.8 in which values for σ_{LN} and $<k>$ at each oscillatory cycle are given by the simulation of the AL model. The bound has the same behavior as the estimated probability. Moreover, it is predictive: the binary code obtained by assigning +1 for phase-locked PNs each time the bound exceeds 0.3 (Wehr & Laurent, 1996) and 0 for nonphase-locked PNs is the same as the one obtained in the simulation of our AL model (see Figure 3).

Figure 6B compares the standard deviation σ_{PN} of the firing times for the PNs computed by using equations 3.8 and 3.9 to the one estimated by simulation. The number of active LNs (N^a_{LN}) and the temporal jitter (σ_{LN})

are similar to the values encountered in the simulations of our AL model in section 2. From Figure 6B we see that $\sigma_{PN} > \sigma_{LN}$ in almost all cases, indicating that PN phase locking requires precise inhibition. Moreover, the close match between theoretical and experimental σ_{PN} values shows that the approximations made in section 3 for deriving equation 3.8 are valid. In the locust AL, the standard deviation of the phase, relative to the LFP oscillations, was found to be 52 degrees for the PNs and 26 degrees for the LNs (Laurent & Davidowitz, 1994). For 20 Hz LFP oscillations, this corresponds to $\sigma_{PN} \approx 7$ ms and $\sigma_{LN} \approx 3.8$ ms, indicated by a star in Figure 6B. The apparent discrepancy between the σ_{PN} value derived from Laurent and Davidowitz (1994) and our results is probably explained by the fact that the mathematical analysis in section 3 did not take into account the PNs that do not receive any inhibition. Therefore, the σ_{PN} values computed with equations 3.8 and 3.9 are likely to be underestimated.

The period of the LFP oscillations is given in equation 3.6, where the mean inhibitory drive is $<k> = p\, N_{LN}^a$, with p the probability of connection and N_{LN}^a the number of active LNs. Because the number of activated glomeruli increases with odor concentration, the percentage of neurons receiving the stimulus reflects the odor concentration (model assumption in section A.1). Therefore, as odor concentration increases, more LNs are active and $<k>$ is higher. From equation 3.6, $\overline{T}$ grows as $\ln <k>$, and thus the frequency of the LFP oscillations should be quite robust to changes in odor concentration. This is indeed verified with simulation results from the AL model presented in Figure 7A. Moreover, as seen in both equation 3.6 and Figure 7A, the period of the LFP oscillation depends linearly on the decay time of the inhibitory synapses. This is in agreement with previous results (e.g., Chow, White, Ritt, & Kopell, 1998). As seen above, the range of inhibitory drive that allows PN phase locking grows with $<k>$, and more PNs are synchronized when $<k>$ increases. Thus, the oscillations of the LFP increase at high concentrations. This is verified in Figure 7B, where the LFP becomes a pure oscillatory signal as the percentage of neurons activated by the stimulus increases.

Figure 6: (A) Lower bound versus estimated phase-locking probability. The solid curve represents the phase-locking probability estimated by simulation over 20 runs (refer to PN#1 in Figure 3). The dotted curve represents the lower bound computed by using equations 3.7 and 3.8. (B) Temporal jitter. Standard deviation σ_{PN} of the firing times for the PN population versus standard deviation σ_{LN} of the firing times for the LN population. Curves represent the σ_{PN} computed using equations 3.9 and 3.8 and section A.2. The mean inhibitory drive is given by $<k> = p\, N_{LN}^a$, with p being the probability of connection and N_{LN}^a being the

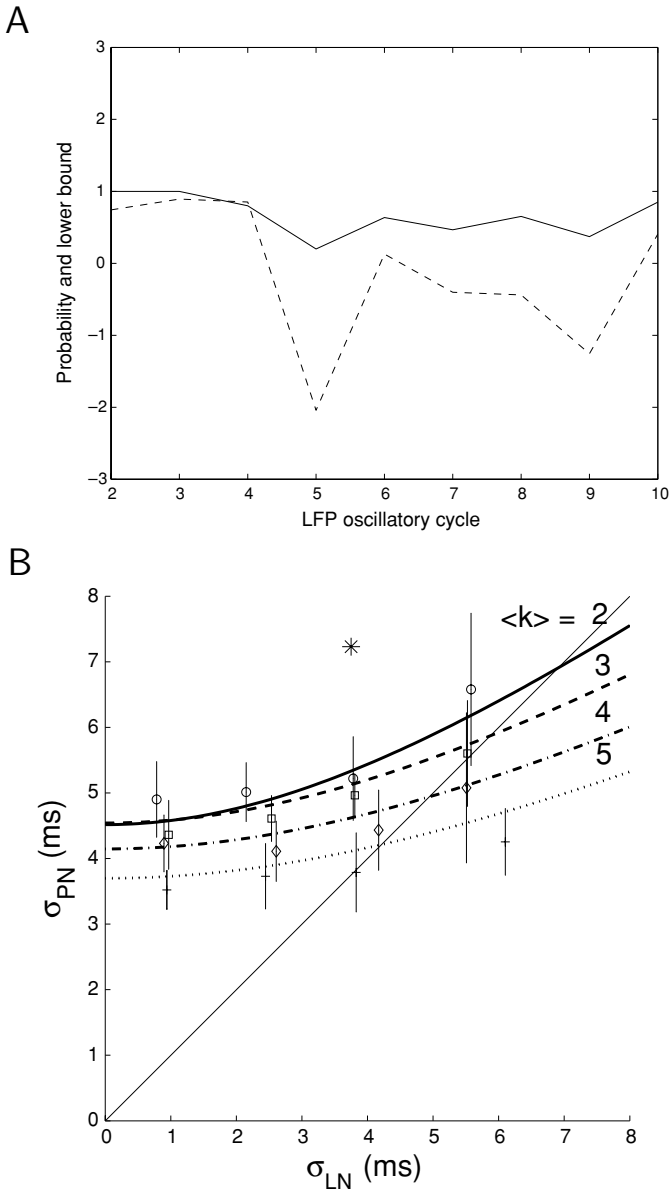

number of active LNs. Points represent experimental values for σ_{PN} estimated as average over 20 runs with standard deviation. Circles, squares, diamonds, and cross marks are for $\langle k \rangle = 2$, 3, 4, and 5, respectively. The value indicated by a star was derived from Laurent & Davidowitz (1994) (see text). The identity line is represented in the graph.

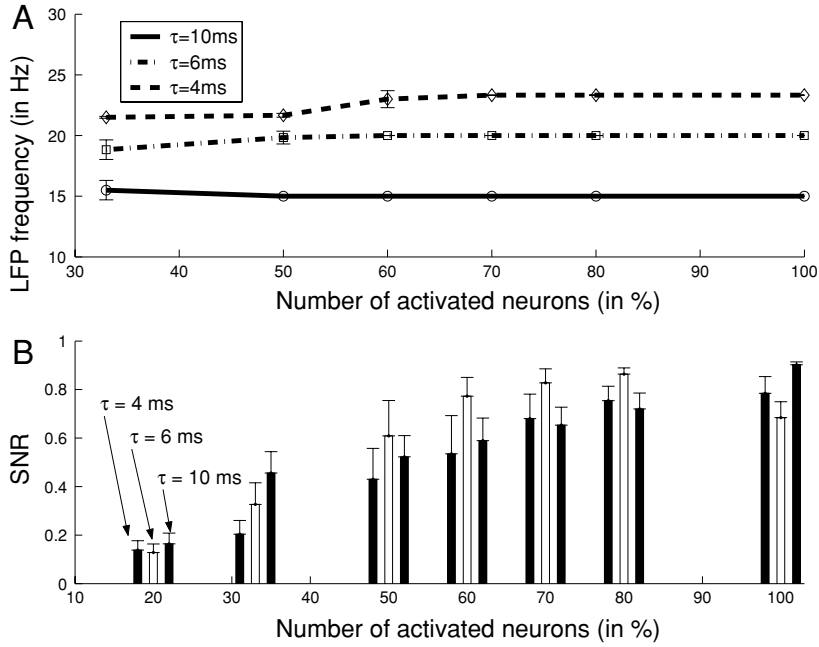

Figure 7: Effects of odor concentration on the LFP. The percentage of neurons activated by the stimulus reflects the odor concentration (model assumption in section A.1). (A) LFP frequency versus odor concentration for different decay rates of the inhibitory LN-PN synapse. The LFP frequency is given by the frequency of the maximum Fourier component in the power spectrum computed on the unfiltered signal. (B) Signal-to-noise ratio (SNR) versus odor concentration. The SNR is defined as the ratio of the sum of the powers of the fundamental and all harmonic frequencies to the total power. The fundamental frequency of the signal is given by the frequency of the maximum Fourier component in the LFP power spectrum. When the SNR is one, the signal is considered a pure oscillatory signal.

5 Discussion

In this article, we outline a mathematical method for predicting PN phase locking from feedback inhibitory input. To the best of our knowledge, this has never been characterized analytically, although both experimental and modeling studies have revealed the relevance of GABAergic inhibition in the synchronization of PNs (MacLeod & Laurent, 1996; Stopfer et al., 1997; Hosler et al., 2000; Bazhenov et al., 2001b). The phase locking probability given by equations 3.7 and 3.8 depends on both the number k and the temporal jitter σ_{LN} of LN-evoked IPSPs. A PN will be phase-locked at the

next oscillatory cycle with probability one if the inhibition received at the current cycle is both perfectly balanced (zero deviation from mean inhibition $k = <k>$) and precise (zero jitter $\sigma_{LN} = 0$).

Precise inhibition is consistent with experimental data from the locust AL for which $\sigma_{LN} < 4$ ms (Laurent & Davidowitz, 1994). Other studies have reported that phase-locked and precisely timed inhibition can be necessary for sensory coding, as in the auditory system (Brand, Behrend, Marquardt, McAlpine, & Grothe, 2002). In the mouse olfactory bulb, however, inhibitory feedback from granule cells (GCs) is not precise. The standard deviation of the normalized phase of the IPSPs received by a mitral cell (MC), relative to the respiratory cyle, was found to be 0.09 (see Figure 6B2 in Margrie & Schaefer, 2003). This corresponds to $\sigma_{GC} \approx 22$ ms (respiration cycle of 250 ms). Despite the jitter in their received IPSPs, MCs exhibit an oscillatory synchronized activity (Kashiwadani, Sasaki, Uchida, & Mori, 1999), and this synchronization is attributed to inhibitory feedback from the GCs (Lagier, Carleton, & Lledo, 2004). From equations 3.7 and 3.8, we see that the temporal jitter σ_{GC} contributes negatively to the MC phase-locking probability through the ratio σ_{GC}^2/k (a small ratio implies higher probability). Because of the large number of GCs in the bulb (in the order of 10^6), the number k of IPSPs received by a particular MC at each oscillatory cycle is expected to be large. Thus, there is no requirement to have precise inhibition (σ_{GC} small) in order for the MCs to be phase-locked. For oscillatory synchronization, the mouse olfactory bulb probably needs to maintain a large number of GCs. As shown in Gheusi et al. (2000), a dramatic reduction in the number of GCs by about 40% leads to impaired odor discrimination. When the number of inhibitory cells is small, as is the case in the locust AL (300 LNs for 830 PNs), oscillatory synchronization requires precise inhibition. In our model, precision of LN firing comes from the phasic nature of excitation resulting from synchronized PNs. Synchronous LN activity can be further reinforced by the use of lateral LN-LN inhibition (see Figure 8D) and by the dense connectivity from PNs to LNs, found to be higher than 80% in Jortner, Mazor, and Laurent (2003).

The phase-locking probability is an asymmetric bell-shaped function centered on the inhibition $<k>$ received on average by the PNs. The inhibition k received by a particular PN is said to be balanced when it does not deviate too much from $<k>$. If a PN receives either a fairly large or a fairly small amount k of inhibition relative to the mean inhibitory drive $<k>$, then it is likely that it will fire very far away from the other PNs. In such a condition, the inhibition is not balanced, and the PN is not phase-locked. The range of k allowing phase locking grows with $<k>$ so that more PNs are expected to be synchronized when more LNs are activated by the stimulus. This finding is in agreement with numerical observations indicating a correlation between the amount of received inhibition and the synchronization of PNs (Bazhenov et al., 2001b). It is also consistent with experimental data showing

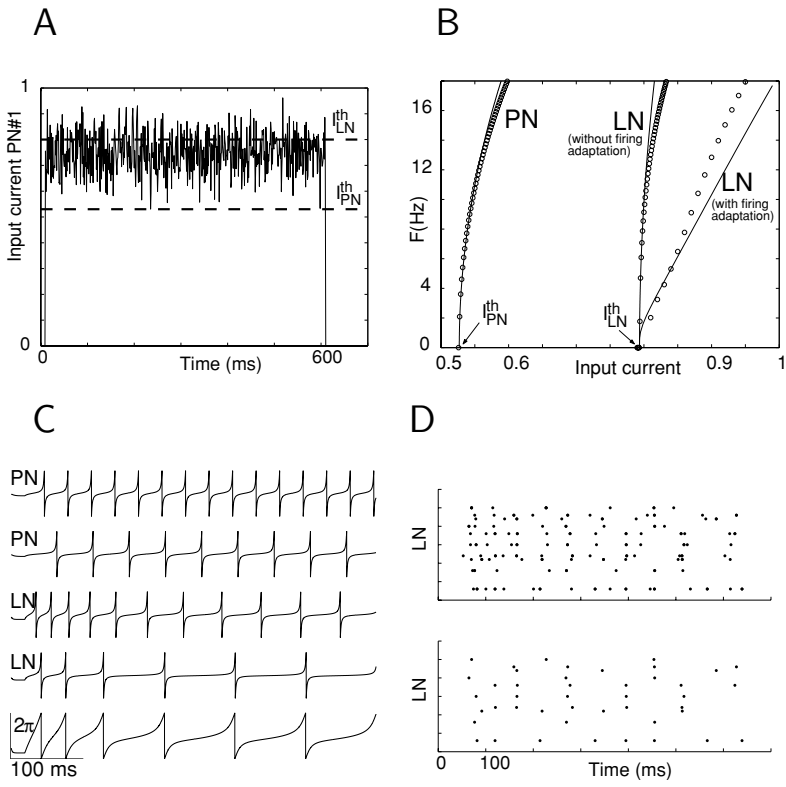

Figure 8: (A) External input. Time evolution of I^{ext} applied to PN #1. $I^{ext} = 0.75$ with added gaussian noise (0.1 standard deviation) of 600 ms duration. Stimulus onset is randomly taken between 0 and 30 ms. The minimal currents I^{th}_{PN} and I^{th}_{LN} necessary for repetitive firing of PNs or LNs are indicated by the dashed lines. (B) Firing rate versus applied current for a PN (left) and a LN (right). Circles are for the simulations of the conductance-based models from Bazhenov et al. (2001b), and plain curves are for the simulations of the corresponding fitted theta models. As expected, theta neurons are a good approximation of type I conductance-based models around the threshold (Ermentrout, 1996; Hoppenstead & Izhikevich, 2002) and firing-rate adaptation linearizes the LN frequency response (Ermentrout, 1998). (C) Responses of PN and LN to current pulses of different amplitude. From top to bottom, $I^{ext} = 0.55, 0.53, 0.85, 0.82,$ and 0.82. Bottom trace was obtained by introducing an additional parameter β in equation 2.1. The result is a more realistic shape for the LN Ca^{2+} spikes, similar to the one in Bazhenov et al. (2001b). (D) Lateral LN-LN inhibition leads to synchronized LN activities even in presence of desynchronized PNs. Raster plots of LN spikes corresponding to the simulation of Figure 2B with LN-LN inhibition (bottom) and without LN-LN inhibition (top).

that both LN and PN oscillatory power increases with odor concentration (Stopfer et al., 2003).

Our mathematical study is based on two basic assumptions. First, we consider only one spike per neuron at each oscillation cycle. This is justified by experimental observations showing that when a PN is phased-locked, it usually produces a single spike per oscillatory cycle (Laurent, 1996; Wehr & Laurent, 1996). Second, we consider PN phase locking as a Markov process so that only information about the inhibition received at the current oscillatory cycle is sufficient for predicting whether a given PN will be phase-locked at the next cycle. This assumption is common and has been already made in more abstract AL models like the DNF (Quenet & Horn, 2003) or the DAL (Holub, Laurent, & Perona, 2002). Both of these AL models consist of networks of binary units with one-step discrete temporal dynamics. A discrete temporal dynamics is consistent with experimental data showing that the firing probability of a PN during a given cycle is coupled to its firing probability in a different cycle of the same trial (Wehr & Laurent, 1996). The Markov assumption is valid for the fast LN-PN inhibition considered in our model because the time constant of the inhibitory synapse (10 ms) is much lower than the period of the LFP oscillation (50 ms). Both experimental and modeling results have shown that PN synchronization is generated by fast GABAergic inhibition, while slow PN temporal patterning comes from another distinct inhibitory mechanism (MacLeod & Laurent, 1996; Bazhenov et al., 2001a). The Markov assumption, however, would not be appropriate for studying slow LN-PN inhibition for which the time constant is much higher than the period of the oscillation.

Appendix: Parameters Used for the AL Model and Probabilities Derived from the Connectivity

A.1 Parameters Used for the AL Model.

A.1.1 Stimulus. The dose response curve of an olfactory glomerulus in insects and mammals has a sigmoid shape (Meister & Bonhoeffer, 2001; Wachowiak & Cohen, 2001; Wang, Wong, Flores, Vosshall, & Axel, 2003; Sachse and Galizia, 2003). For simplicity, we consider a binary glomerular response (active or inactive) as in (Ng et al., 2002). In the insect AL, both PNs and LNs receive inputs from the glomeruli. Because the number of activated glomeruli increases with odor concentration (Ng et al., 2002; Sachse & Galizia, 2003), the percentage of neurons in our network receiving the external input mimics odor concentration. Unless otherwise specified, the input is applied to 33% of the neurons chosen at random. For each of these activated neurons, the input consists of a constant current $I^{ext} = 0.75$ with added gaussian noise (0.1 standard deviation) of 600 ms duration (stimulus onset randomly chosen between 0 and 30 ms) (see Figure 8A).

4.1.2 Neurons. In the locust, PNs fire classical sodium action potentials, but LNs do not. When stimulated by a constant current, LNs produce calcium-like spikelets whose frequency decreases during the duration of the stimulation (Laurent, Seymour-Laurent, & Johnson, 1993). We simulated the conductance-based models of PNs and LNs from Bazhenov et al. (2001b) and found that their firing frequency in response to a constant input current can be arbitrarily low (type I excitability). In order to reduce complexity, we choose to use the quadratic integrate-and-fire model or the equivalent nondiverging theta model, both of which are known to be very good approximations of any type I neuron around the threshold (Ermentrout, 1996; Hoppenstead & Izhikevich, 2002). The equation for the theta neuron is given by equation 2.1, where the total input current is

$$J = I - I^{adapt} + I^{syn}.$$

$I = I^{ext} - I^{th}$ where I^{ext} is the external current and I^{th} denotes the threshold, the minimal current required for repetitive firing. I^{adapt} and I^{syn} are the adaptation and synaptic current, respectively. Parameters α and I^{th} of the theta neurons have been fitted so as to obtain the same frequency-current response as their equivalent conductance-based neuron without firing-rate adaptation (see Figure 8B). PNs and LNs have a threshold of 0.53 and 0.79, respectively, which means that the LNs are less excitable than the PNs. The constant α was 0.05 for a PN and 0.1 for a LN. In Bazhenov et al. (2001b), the LN has an adaptation current, but the PN does not. We therefore introduced in our LN theta model a slow adaptation current whose form was given by Izhikevich (2000). For PNs, $I^{adapt} = 0$. For LNs, I^{adapt} increases of a fixed step equal to 0.05 whenever the cell fires and then relaxes exponentially toward zero with a decay rate of 200 ms. The frequency-current response of the adapting LN is shown in Figure 8B, and responses of PN and LN to current pulses of different amplitude are shown in Figure 8C. A more realistic shape for the LN Ca^{2+} spikes, similar to the one in Bazhenov et al. (2001b), can be obtained by introducing an additional parameter β such that equation 2.1 becomes $d\theta/dt = (1 - \cos\theta)\beta + (1 + \cos\theta)\alpha J$. When $J > 0$ and is constant, the firing frequency is given by $\sqrt{\alpha\beta J}/\pi$, while the spike width can be adjusted by the ratio α/β (see the bottom trace in Figure 8C and Börgers & Kopell, 2003, for a discussion about the spike width in the theta neuron). However, because simulation results were not dependent on a particular shape of the LN spikes, the simpler LN model given by equation 2.1 was used.

4.1.3 Network. The AL network is a sparsely and randomly connected network with the same probability $p = 0.5$ of connection from LNs to PNs, PNs to LNs, and between LNs. We did not consider interconnections

between PNs because they seem to have a negligible influence in the original model of Bazhenov et al. (2001b). Neurons are coupled via simple exponential synapses. When two neurons are connected, the connection strength is 0.05 between a PN and a LN, -0.5 between a LN and a PN, and -0.1 between two LNs. The time constant is 5 ms and 10 ms for the excitatory and inhibitory synapse, respectively.

A.2 Probability That an Inhibited PN Receives Exactly k Inhibitions. In the presence of a stimulus, the number of active LNs changes over time (see e.g., Figure 2A). Let N_{LN}^a be the number of LNs that are active at the current LFP oscillation and p the probability of connection from LNs to PNs ($p = 0.5$ for the AL model). Then the probability that a PN receives k inhibitions from the LNs with $k \geq 0$ is simply given by the binomial distribution with parameters N_{LN}^a and p,

$$P_{PN}(X = k) = \binom{N_{LN}^a}{k} \; p^k (1-p)^{N_{LN}^a - k}.$$

The probability that an inhibited PN receives exactly k inhibitions with $k \geq 1$ is actually a conditional probability that can be found using the Bayes' rule,

$$p_k = P_{PN}(X = k | k \geq 1) = \frac{P_{PN}(X = k)}{1 - P_{PN}(X = 0)}.$$

A.3 Firing Probability for a KC Receiving PN Spikes Within a ± 5 Ms Window. Experimental observations suggest that PN spikes occur within a 5 ms window when they are phase-locked (Laurent, 1999). In order to check if this value could be used for estimating the lower bound, we have simulated a conductance-based model of a KC given in Ikeno and Usui (1999) with k input spikes generated with a uniform distribution in a $\epsilon = \pm 5$ ms window. The synaptic currents have been modeled as double exponentials with parameter values (peak current, decay, and rise time constants) given in Su and O'dowd (2003). The conditional probability for the KC to fire given k input spikes phase-locked at $\epsilon = \pm 5$ ms has been estimated as the average over 200 runs, which gives $Pf(k) = 0$ for $k < 3$, $Pf(3) = 0.79$, and $Pf(k) = 1$ for $k > 3$. Assuming n_{KC} random connections from the PNs, the probability for a KC of receiving such phase-locked k PN spikes is given by the binomial distribution

$$P(k) = \binom{n_{KC}}{k} \; P_{PN}^k (1 - P_{PN})^{n_{KC} - k},$$

where P_{PN} is the probability of a PN to be phase-locked. Finally, the probability of a KC to fire is simply

$$P_{KC} = \sum_{k=0}^{n_{KC}} P(k) Pf(k).$$

We consider $n_{KC} = 15$ (it is known that $10 \leq n_{KC} \leq 20$ for the locust), $P_{PN} \approx 0.1$ (Wehr & Laurent, 1996) and $Pf(k)$ estimated as above for $\epsilon = \pm 5$ ms. We find $P_{KC} = 0.16$, which is in agreement with the KC response probability of 0.1 found experimentally in Perez-Orive et al. (2002). Therefore, $\epsilon = \pm 5$ ms appears to be a correct value for determining if a PN is phase-locked.

Acknowledgments

This work was supported by a Cooperative Research Initiative from INRIA and by the European Network of Excellence GOSPEL (General Olfaction and Sensing Projects on a European Level).

References

Bazhenov, M., and Stopfer, M., Rabinovich, M., Abarbanel, H., Sejnowski, T., & Laurent, G. (2001a). Model of cellular and network mechanisms for odor-evoked temporal patterning in the locust antennal lobe. *Neuron*, *30*, 569–581.

Bazhenov, M., Stopfer, M., Rabinovich, M., Huerta, R., Abarbanel, H., and Sejnowski, T., & Laurent, G. (2001b). Model of transient synchronization in the locust antennal lobe. *Neuron*, *30*, 553–567.

Börgers, C., & Kopell, N. (2003). Synchronization in networks of excitatory and inhibitory neurons with sparse, random connectivity. *Neural Computation*, *15*, 509–538.

Brand, A., Behrend, O., Marquardt, T., McAlpine, D., & Grothe, B. (2002). Precise inhibition is essential for microsecond interaural time difference coding. *Nature*, *417*, 543–547.

Buzsaki, G., & Draguhn, A. (2004). Neuronal oscillations in cortical networks. *Science*, *304*, 1926–1929.

Chow, C., White, J., Ritt, J., & Kopell, N. (1998). Frequency control in synchronized networks of inhibitory neurons. *Journal of Computational Neuroscience*, *5*, 407–420.

Ermentrout, B. (1996). Type 1 membranes, phase resetting curves, and synchrony. *Neural Computation*, *8*, 979–1001.

Ermentrout, B. (1998). Linearization of F-I curves by adaptation, *Neural Computation*, *10*, 1721–1729.

Friedrich, R., Habermann, C., & Laurent, G. (2004). Multiplexing using synchrony in the zebrafish olfactory bulb. *Nature Neuroscience*, *7*, 862–871.

Gheusi, G., Cremer, H., McLean, H., Chazal, G., Vincent, J.-D., & Lledo, P.-M. (2000). Importance of newly generated neurons in the adult olfactory bulb for odor discrimination. *PNAS*, *97*, 1823–1828.

Holub, A., Laurent, G., & Perona, P. (2002). A digital antennal lobe for pattern equalization: Analysis and design. In S. Becker, S. Thrün, & K. Obermayer (Eds.), *Advances in neural information processing systems*, *15*. Cambridge, MA: MIT Press.

Hoppenstead, F., & Izhikevich, E. (2002). *Canonical neural models in brain theory and neural networks* (2nd ed.). Cambridge, MA: MIT Press.

Hosler, J., Buxton, K., & Smith, B. (2000). Impairment of olfactory discrimination by blockade of GABA and nitric oxide activity in the honey bee antennal lobes. *Behavioral Neuroscience*, *114*, 514–525.

Huxter, J., Burgess, N., & O'Keefe, J. (2003). Independent rate and temporal coding in the hippocampal pyramidal cells. *Nature*, *425*, 828–832.

Ikeno, H., & Usui, S. (1999). Mathematical description of ionic currents of the Kenyon cell in the mushroom body of honeybee. *Neurocomputing*, *26–27*, 177–184.

Izhikevich, E. (2000). Neural excitability, spiking and bursting. *International Journal of Bifurcation and Chaos*, *10*, 1171–1267.

Jortner, R., Mazor, O., & Laurent, G. (2003). Local connectivity in the locust antennal lobe. In *Proceedings of the Computational Neuroscience Meeting*, CNS 2003 (p. 100). Alicante, Spain.

Kashiwadani, H., Sasaki, Y., Uchida, N., & Mori, K. (1999). Synchronized oscillatory discharges of mitral/tufted cells with different molecular receptive ranges in the rabbit olfactory bulb. *Journal of Neurophysiology*, *82*, 1786–1792.

Kopell, N. (2003). We got rhythm: Dynamical systems of the nervous system. *Notices of the AMS*, *47*, 6–16.

Lagier, S., Carleton, A., & Lledo, P.-M. (2004). Interplay between local GABAergic interneurons and relay neurons generate γ oscillations in the rat olfactory bulb. *Journal of Neuroscience*, *24*, 4382–4392.

Laurent, G. (1996). Dynamical neural assemblies, *TINS*, *19*, 489–496.

Laurent, G. (1999). A systems perspective on early olfactory coding. *Science*, *286*, 723–728.

Laurent, G., & Davidowitz, H. (1994). Encoding of olfactory information with oscillating neural assemblies. *Science*, *265*, 1872–1875.

Laurent, G., Seymour-Laurent, K., & Johnson, K. (1993). Dendritic excitability and a voltage-gated calcium current in locust nonspiking local interneurons. *Journal of Neurophysiology*, *69*, 1484–1498.

Laurent, G., Stopfer, M., Friedrich, R., Rabinovich, M., Volkovskii, A., & Abarbanel, H. (2001). Odor coding as an active, dynamical process: Experiments, computation and theory. *Annu. Rev. Neurosci.*, *24*, 263–297.

Laurent, G., Wehr, M., & Davidowitz, D. (1996). Temporal representations of odors in an olfactory network. *Journal of Neuroscience*, *16*, 3837–3847.

MacLeod, K., & Laurent, G. (1996). Distinct mechanisms for synchronization and temporal patterning of odor-encoding neural assemblies. *Science*, *274*, 976–979.

Margrie, T., & Schaefer, A. (2003). Theta oscillation coupled spike latencies yield computational vigour in a mammalian sensory system. *Journal of Physiol.*, *546*, 363–374.

Meister, M., & Bonhoeffer, T. (2001). Tuning and topography in an odor map on the rat olfactory bulb. *Journal of Neuroscience*, *21*, 1351–11360.

Ng, M., Roorda, R., Lima, S., Zemelman, B., Morcillo, P., & Miesenbock, G. (2002). Transmission of olfactory information between three populations of neurons in the antennal lobe of the fly. *Neuron*, *36*, 463–474.

O'Keefe, J. (1993). Phase relationship between hippocampal place units and the EEG theta rhythm. *Hippocampus*, *3*, 317–330.

Papoulis, A. (1984). *Probability, random variables, and stochastic processes* (2nd ed.). New York: McGraw-Hill.

Perez-Orive, J. (2004). *Neural oscillations and the decoding of sensory information*. Unpublished doctoral dissertation, California Institute of Technology.

Perez-Orive, J., Mazor, O., Turner, G., Cassenaer, S., Wilson, R., & Laurent, G. (2002). Oscillations and sparsening of odor representations in the mushroom bodies. *Science*, *297*, 359–365.

Quenet, B., & Horn, D. (2003). The dynamic neural filter: A binary model of spatiotemporal coding. *Neural Computation*, *15*, 309–329.

Sachse, S., & Galizia, C. (2003). The coding of odour-intensity in the honeybee antennal lobe: Local computation optimizes odour representation. *European Journal of Neuroscience*, *18*, 2119–2132.

Stopfer, M., Bhagavan, S., Smith, B., & Laurent, G. (1997). Impaired odor discrimination on desynchronisation of odor-encoding neural assemblies. *Nature*, *390*, 70–74.

Stopfer, M., Jayaraman, V., & Laurent, G. (2003). Intensity versus identity coding in the olfactory system. *Neuron*, *39*, 991–1004.

Su, H., & O'Dowd, D. (2003). Fast synaptic currents in drosophila mushroom body Kenyon cells are mediated by α-bungarotoxin-sensitive nicotinic acetylcholine receptors and picrotoxin-sensitive GABA receptors. *Journal of Neuroscience*, *23*, 9246–9253.

Wachowiak, M., & Cohen, L. (2001). Representation of odorants by receptor neuron input in the mouse olfactory bulb. *Neuron*, *32*, 723–735.

Wang, J., Wong, A., Flores, J., Vosshall, L., & Axel, R. (2003) Two-photon calcium imaging reveals an odor-evoked map of activity in the fly brain. *Cell*, *112*, 271–282.

Wang, X.-J. (2003). Neural oscillations. In L. Nadel (Ed.), *Encyclopedia of cognitive science* (pp. 272–280). New York: MacMillan.

Wang, X.-J., & Buzsaki, G. (1996). Gamma oscillation by synaptic inhibition in a hippocampal interneuronal network model. *Journal of Neuroscience*, *16*, 6402–6413.

Wehr, M., & Laurent, G. (1996). Odour encoding by temporal sequences of firing in oscillating neural assemblies. *Nature*, *384*, 162–166.

Whittington, M., Traub, R., Kopell, N., Ermentrout, B., & Buhl, E. (2000). Inhibition-based rhythms: Experimental and mathematical observations on network dynamics. *Int. J. of Psychophysiol.*, *38*, 315–336.

Received November 17, 2004; accepted April 26, 2005.